# MWA Array Layout

Adam Beardsley[1], Bryna Hazelton, Miguel Morales

**Abstract**

The Murchison Widefield Array (MWA) will consist of 512 "tiles" (each comprised of 16 radio dipoles). Placing these tiles to best suit the science goals of the MWA becomes a difficult problem when constraints such as avoiding vegetation, flood regions, and bedrock are taken into account. We develop a Figure of Merit for quantitatively comparing different array realizations, which accurately describes the similarity between a given sample array and the ideal array. Then we describe a method for actively selecting tile locations in order to minimize the Figure of Merit, and maximize the azimuthal symmetry in the baseline distribution of the array. These methods can be used to determine the final MWA array layout to be built in Western Australia.

## 1 Introduction

The Murchison Widefield Array (MWA) is a low frequency radio interferometer under construction in the Western Australia Outback. The primary science goals of the MWA are detection of the 21 cm neutral hydrogen line from the Epoch of Reionization (EOR), measurements of the Sun and the heliospheric plasma, and a high sensitivity survey of the dynamic radio sky. It will consist of 8192 dipoles, arranged into 512 "tiles". The majority of the tiles (496) will be distributed throughout a 1.5km diameter core, with the remaining 16 tiles at a 3km diameter to provide longer baselines, and thus higher angular resolution, for solar measurements. The tile density distribution will be constant within a central 75m radius, and have a $r^{-2}$ dependence beyond. With a normalization of 496 tiles, this results in an ideal central density of 5000 tiles/km$^2$. Receivers will also be placed in the field, serving 8 tiles each.

Due to the nature of an interferometric measurement, the baselines are more important than the physical placement of the antennas. Hence, the array should match the ideal *baseline* distribution as closely as possible. It is also important to note that an ideal distribution is impossible to obtain due to the finite number of discrete tiles. This creates the need for a figure of merit to distinguish the quality of different realizations. In Section 3 we qualitatively compare a small sample of baselines distributions in order to gain intuition on the quality of these realizations. Then we quantify these comparisons in Section 4. Finally, we describe a new algorithm for generating arrays in Section 5.

[1]beards@u.washington.edu

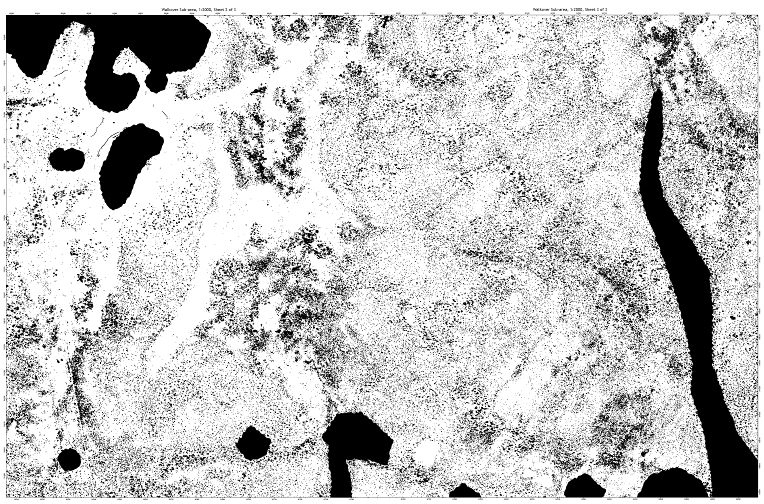

Figure 1: The bitmask used to impose physical constraints on the placement of tiles. Physical locations are converted to correspoding pixels, then checked against the mask. If the pixel is black, the location is thrown out and another is selected.

# 2 Constraints and Definitions

Work has been done to optimize array layouts by taking into account imaging performance and cable length [1]. Our work focuses on meeting scientific demands with the addition of physical constraints at the cite of the array. Future work will address the issue of cable length running to the tiles. When placing tiles, we must be certain not to place any tiles on top of one another. This was avoided by enforcing a minimum distance of 7.5m between any two tiles. Constraints also exist such as avoiding vegetation, flood regions, and bedrock. These constraints are imposed by the use of a bitmask (Figure 1)[2]. This mask was created by the use of an aerial photo, with avoidance areas marked with a black pixel (value of 1), and all other areas marked white (0). This provides an easy boolean check for any possible tile location. Throughout this paper we refer to both “masked” and “unmasked” realizations. This simply refers to whether the bitmask was taken into account, or if all locations were considered valid for tile placement.

We explored a random tile placement algorithm, in which tiles were randomly placed with a weighted distribution, as well as a more active algorithm which will be discussed in Section 5. The output of these algorithms is a list of coordinates for 496 tiles to be placed in the field. We ran these algorithms 500 times each, but in the end a single realization must be chosen to use in the field. As a tool for looking at array realizations, we plot the baseline distribution as well as the difference from the ideal distribution (See Figures 3 - 5). The ideal

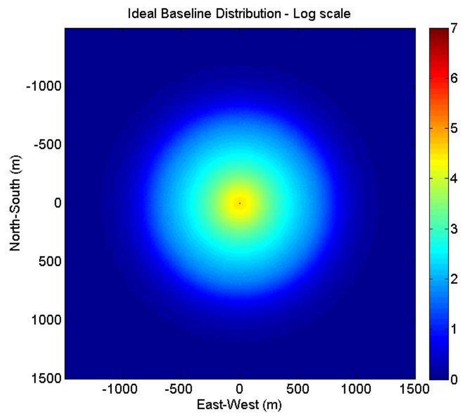


Figure 2: The ideal baseline distribution created by averaging 500 randomly created realizations without the use of a bitmask.

distribution was obtained by running the random algorithm 500 times with no mask, and averaging the baselines (Figure 2). This provides an essentially continuous distribution free from azimuthal asymmetries. The difference functions, $D(r, \phi)$, describe the difference from ideal, and ultimately we wish to rate the merit of the array realizations based on these functions.

# 3 Qualitative Comparisons

Figures 3, 4, and 5 show a few examples of array realizations produced by a random unmasked method, a random masked method, and our new Active Masked method respectively. The left pane in each figure shows the baseline distribution for the given array, on a log scale. The right pane shows the difference between the given array and the ideal array, $D(r, \phi)$. For illustrative purposes, we shall compare the bottom images in Figures 4 and 5.

Both of these images have significant small scale noise, which is much more evident in the right panes. This is due to a type of shot noise. The ideal distribution was created by averaging 500 realizations, while each individual sample realization only consists of 496 discrete tiles. This relatively small number of discrete objects creates the fuzzy noise seen on both these arrays. In fact, this noise is present in all array realizations, and is unavoidable given the specifications of the MWA (496 tiles in the 1.5km core).

However, there is another type of noise present in the bottom image of Figure 4, but essentially absent in the bottom image of Figure 5. This is the large scale azimuthal structure. In most array realizations there are large regions of over and under densities in the baseline distribution. This type of noise is harmful to the quality of the array layout. An asymmetry in the baseline dis-

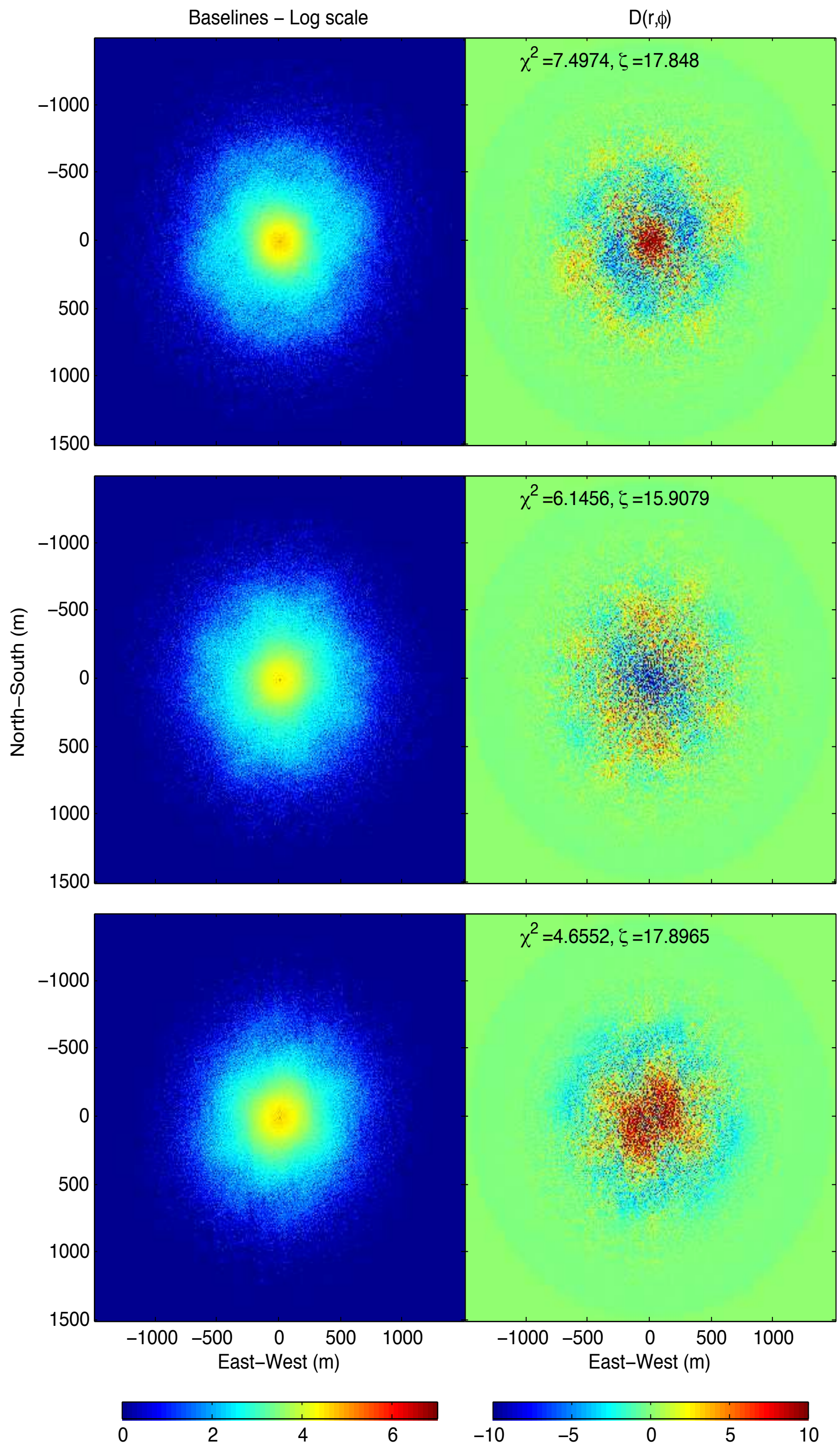


Figure 3: Sample Random Unmasked UV Distributions. These are three randomly selected array realizations created using the random method with no bit mask. Despite not using a mask, some randomly introduced azimuthal asymmetry is visible.

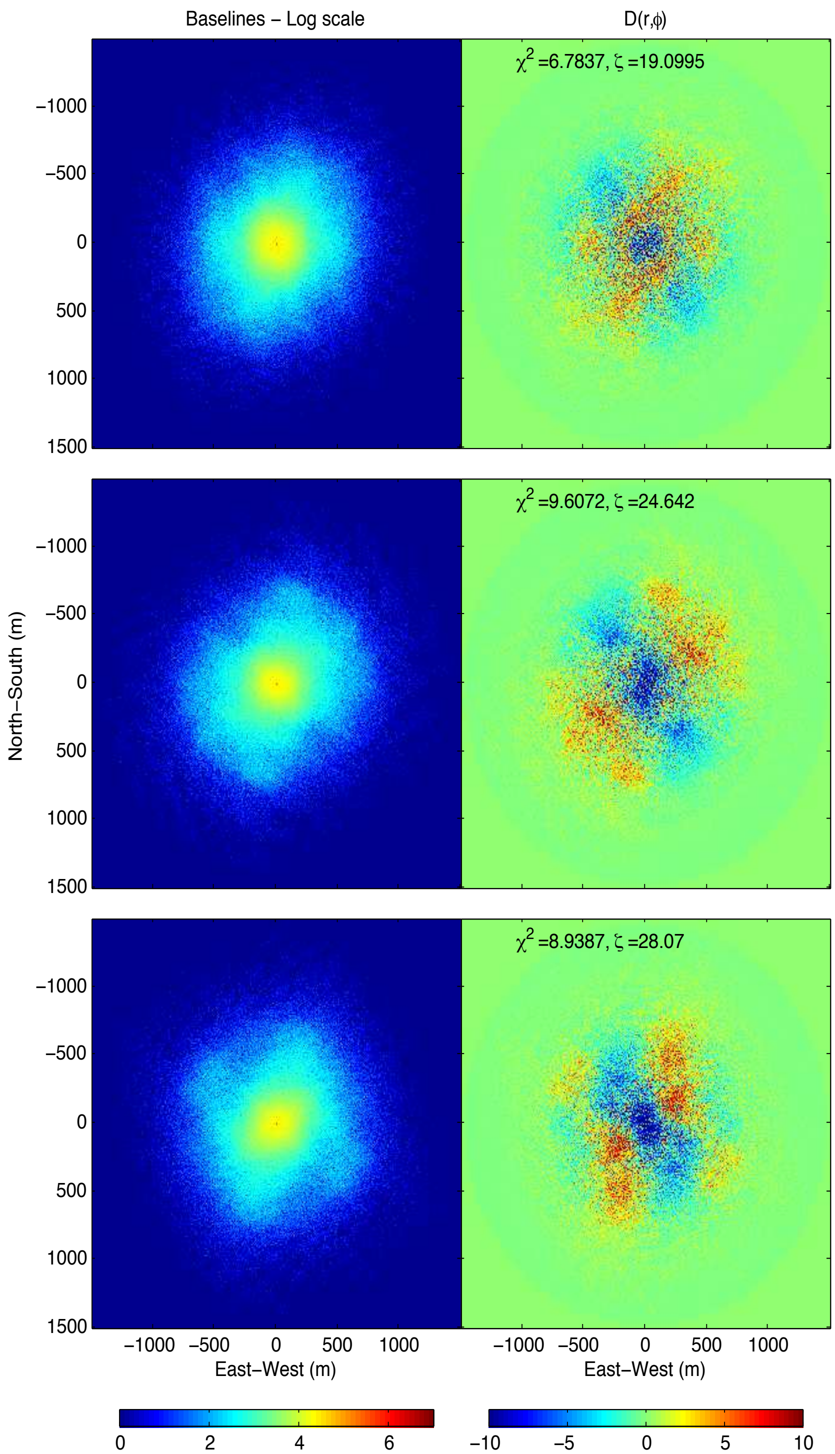


Figure 4: Sample Random Masked UV Distributions. These are three randomly selected array realizations created using the random method with the bit mask (Figure 1).

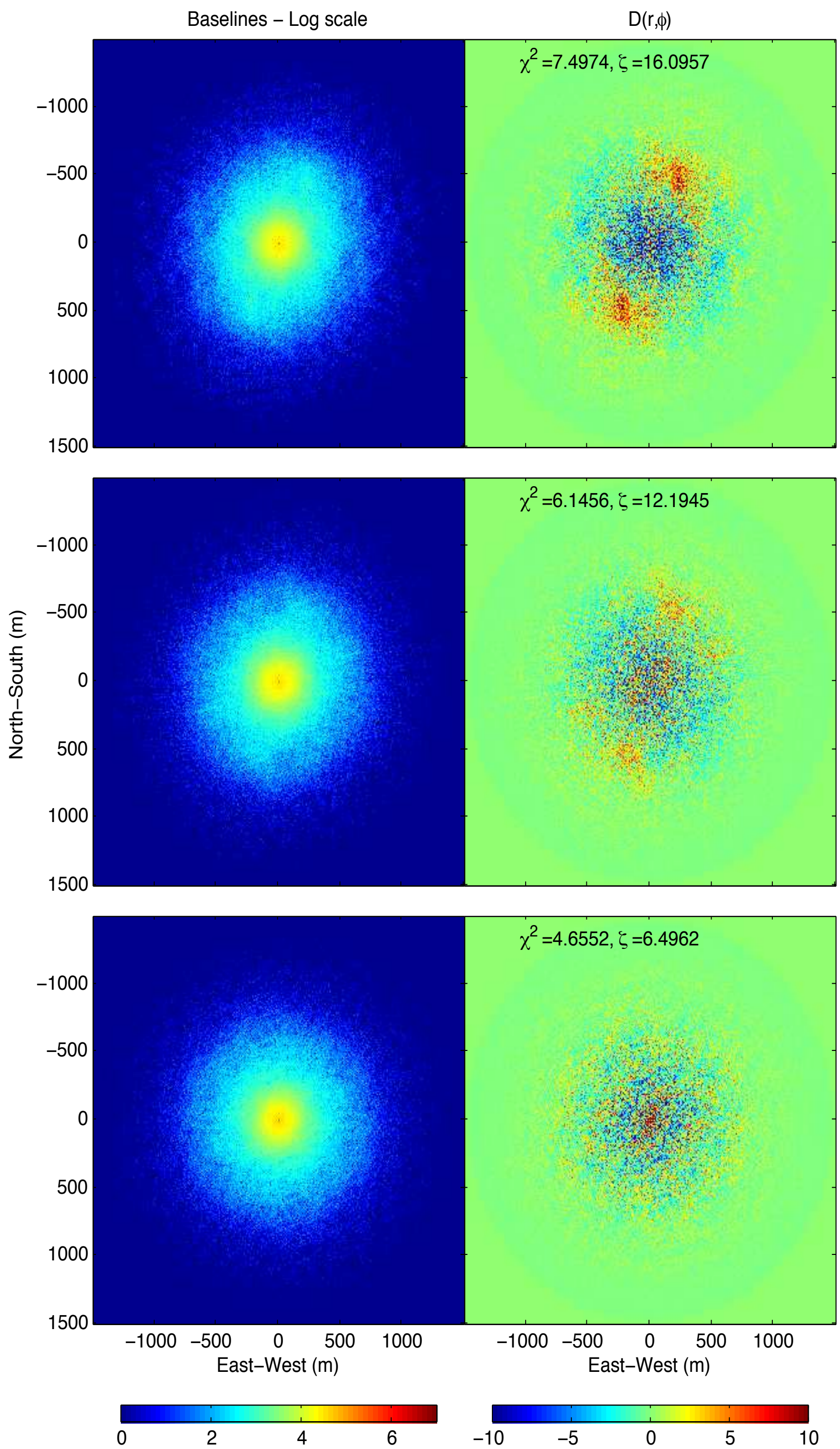




Figure 5: Sample Active Masked UV Distributions. These are three randomly selected array realizations created using the active algorithm described in Section 5 with the bit mask. The large scale azimuthal asymmetry is greatly surpressed in the bottom two realizations.

tributions results in an asymmetry in the point spread function, which infringes on the scientific demands of the MWA. It is in the interest of the scientific goals to minimize this azimuthal asymmetry in the final array layout. As a useful exercise, the reader may want to qualitatively compare each of the example distributions provided, and rank them according to the overall quality of the array. We found as a general trend, the random masked method produced the least azimuthally symmetric distributions, while the Active Masked method produced the most azimuthally symmetric distributions. In the following section, we quantify the noise of the baseline distributions, and describe our Figure of Merit for ranking the arrays.

It is of interest to note that the large scale azimuthal asymmetry arises even in the unmasked random array realizations. With this method, tiles are placed completely randomly (with a weighted radial distribution). Initially one would expect there to be little azimuthal structure. However, this is not the case. It is clear from Figure 3 that this structure does exist in these arrays. This can be understood by considering the affect of a single tile on the baseline distribution. Moving a single tile on the physical ground changes $\approx$1000 baselines in the UV plane. Hence any small deviation from symmetry on the ground is amplified in the UV plane. Due to the finite number of discrete tiles, one should expect some asymmetry in the tile layout, and thus should not be surprised by the large scale structure in the random baseline distribution, even in the unmasked case.

# 4 Quantitative Comparisons

It is now necessary to quantify the significance of the noise in array realizations. We must be able to reduce all the information into a single Figure of Merit in order to rate the realizations, and eventually choose the best one to build.

The first approach is to consider $\chi^2$, which captures the average deviation from ideal (See the appendix for a detailed description of the calculations). However, $\chi^2$ is not a spatially aware function. In other words, any deviation from the ideal is weighted the same, regardless of where in the distribution the deviation occurs. Because of this lack of spatial information, $\chi^2$ does not capture the large scale azimuthal structure that is important to choosing an array. The example realizations in Figures 3 - 5 clearly vary quite a bit in quality. However, the $\chi^2$ values associated with them do not reliably reflect the degree of angular structure. The inability of $\chi^2$ to capture array quality is demonstrated again in the histogram in Figure 6(a). Despite a clear visual difference between arrays generated by the random unmasked and masked methods, the distributions of $\chi^2$ are nearly indistinguishable.

With the angular dependence in mind, our next step was to use a Bessel decomposition to describe the array realizations[3]. This allows us to describe the difference from ideal in a spatially sensitive manner. In particular, we are interested in the power in the $m > 0$ modes, where $m$ denotes the angular mode (Appendix A). The $m = 0$ mode is neglected because it is azimuthally symmet-

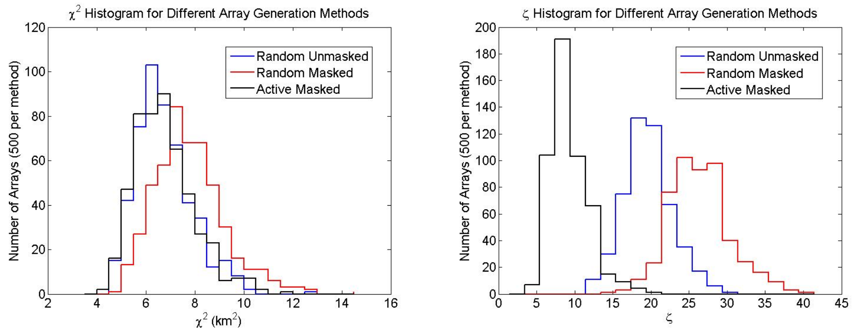


Figure 6: $\chi^2$ and $\zeta$ histograms for 500 array realizations using random and active methods. While the $\chi^2$ values do not distinguish the quality of the different methods, the $\zeta$ values strongly separate the realizations based on azimuthal symmetry.

ric, which is exactly what we are aiming for in the baseline distribution. We define a value, $\zeta$, as the total power in these non-zero modes. This now provides us with a characteristic value which is coupled to the azimuthal structure in the baseline distribution. Refering once again to Figures 3 - 5, we can now see that the $\zeta$ values accurately describe the degree of large scale azimuthal structure present in the sample arrays.[2] This means that $\zeta$ is indeed the correct Figure of Merit to use when discussing the quality of array realizations.

Figure 6(b) demonstrates the ability of $\zeta$ to distinguish the different methods used. In this histogram, we see a clear separation of the three methods, which reflects our qualitative comparisons. The random masked distributions tend to have significantly higher $\zeta$ values than the random unmasked distributions, as expected. The Active Masked method which will be described below actually outperforms the random *unmasked* method in that is creates much more azimuthally symmetric array realizations than can be done in a purely random way.

The attentive reader may notice that the top image in Figure 5 seems to have a substantial amount of asymmetry, despite being produced by the Active Masked method. However, the $\zeta$ value associated with this array shows that it is in fact an outlier of this method's distribution, and lies in the bulk of the random unmasked distribution. In other words, $\zeta$ has successfully marked this particular realization as having significant azimuthal asymmetry. This is further evidence that $\zeta$ is an unbiased Figure of Merit.

[2] These figures are a representative subset of the distributions we examined. The interested reader is encouraged to contact the authors for a larger set of distributions to compare.

# 5 The Active Tile Placement Algorithm

Here we describe the basis for the Active Masked method. This method was created with the goal of minimizing our Figure of Merit, $\zeta$. Because moving an individual tile moves $\approx$1000 baselines, the problem is very non-linear. We approach the problem by going back and forth between the physical tile distribution and the UV plane as we place the tiles.

First we place 350 tiles using the random masked method. Then for each remaining tile, we first choose a random radius, and many candidate azimuthal locations. The number of candidate locations is dependent on the radius. In our analysis, we grid the tiles at 10m spacing, so the effective number of distinct locations is approximately $2\pi r/(10m)$. This is the number of angles we consider. For each candidate location, we calculate the baseline distribution, and an interim $\zeta$ value. We then choose the location with the smallest $\zeta$ value. We proceed in this fashion until all 496 tiles are placed.

The result is clear in Figures 5 and 6(b). When compared to the random unmasked method, despite having the additional constraint of the bitmask, the Active Masked method produces more symmetric baseline distributions.

Using the above method, we created 500 array realizations. Then, using $\zeta$ as our criterion for quality, we easily picked out the best array. Figure 7 shows the baseline distribution of this array. There is essentially no azimuthal asymmetry in this realization. Pending the result of a geological survey, the constraints on the array may change. This would result in a modified bitmask, which can be used to run the Active Masked algorithm again to produce the final array for construction in Western Australia. However, if the constraints do not change upon receiving the results of the survey, the array in Figure 7 is a strong candidate for the final array. Figure 8 shows an aerial photo with the array and sample receiver placements superimposed.

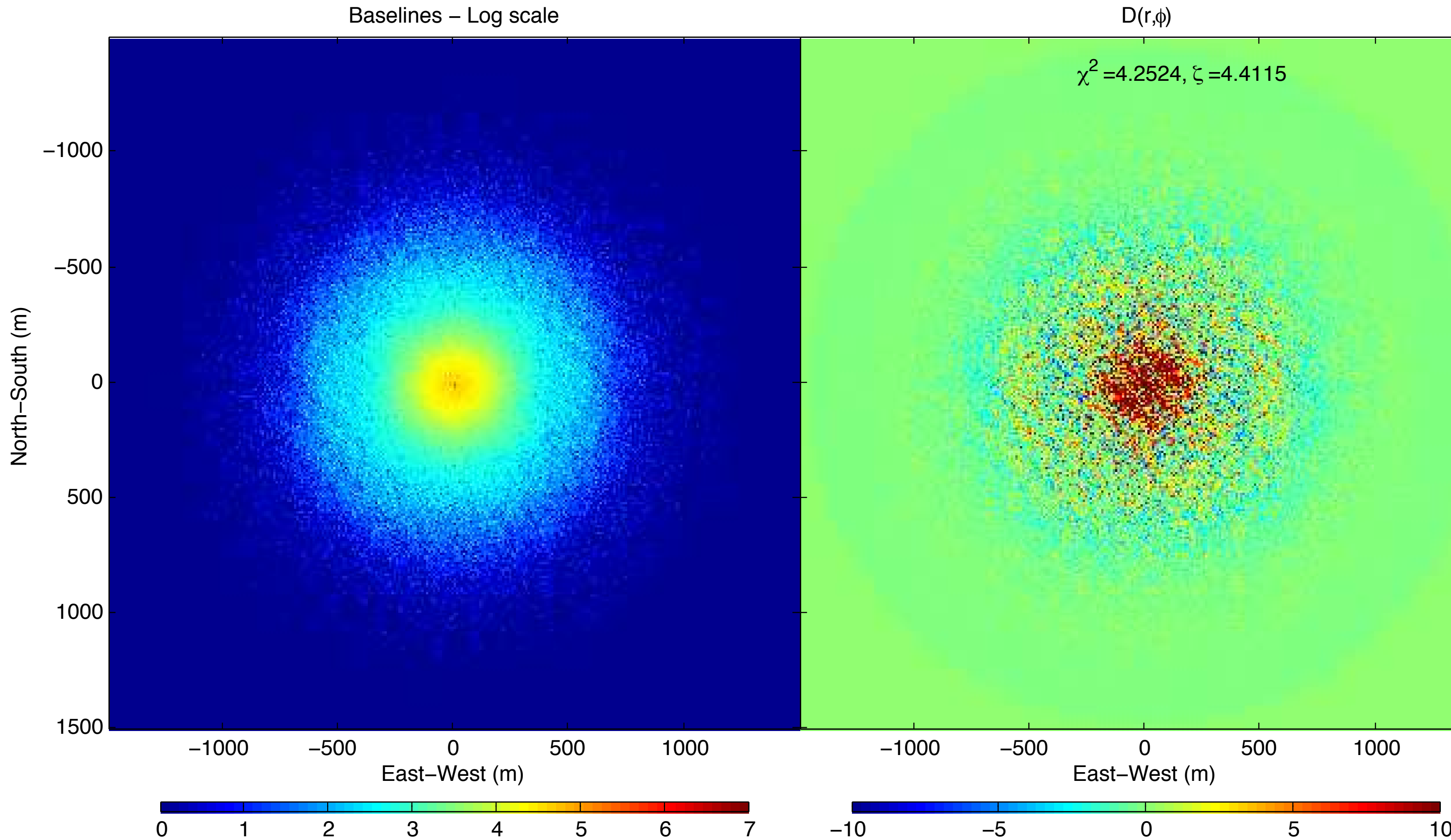


Figure 7: This baseline distribution represents the best array realization we have produced using the Active Algorithm described in Section 5. The array with the smallest $\zeta$ value was selected, and the azimuthal symmetry here suggests that $\zeta$ is indeed a good measure for the quality of the realizations.

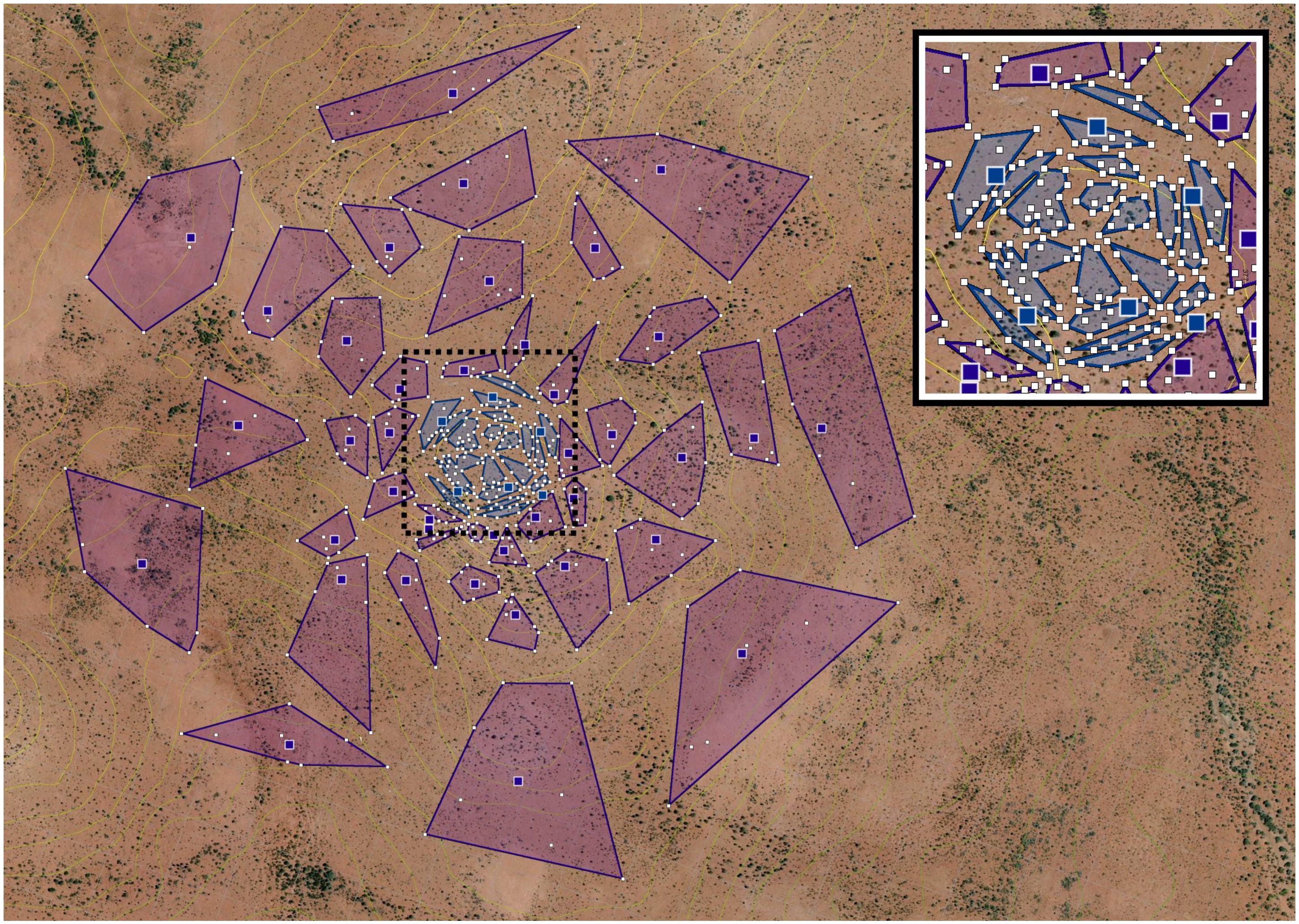

Figure 8: An aerial photo of the MWA site with the same array as in Figure 7 superimposed, with sample receiver placements. White squares represent tiles, blue and purple squares represent receivers. The polygons surround all tiles associated with a given receiver. Inset: An enlarged view of the center of the array.

## 6 Conclusion

We have demonstrated the validity of $\zeta$ as a useful Figure of Merit in distinguishing the quality of array realizations, which can be used to determine the final MWA array layout to be built in Western Australia. By minimizing $\zeta$, we developed an algorithm to generate array realizations which are significantly better than random tile placement, in that they are more azimuthally symmetric. Once a final bitmask is generated using the results of a geological survey, our algorithm can be used to generate a selection of array realizations, from which we can choose a final array by minimizing $\zeta$. Further work is being done to address the issue of receiver placement, and will be discussed in our next memo in this series.

## 7 Acknowledgments

Thank you to Roger Cappallo for providing a jumping off point with the random masked algorithm, and to Colin Lonsdale for generating the bitmask used in our work.

## References

[1] B. Cohanim, J. Hewitt, O. de Weck, "The Design of Radio Telescope Array Configurations using Multiobjective Optimization: Imagin Performance versus Cable Length," Eprint arXiv:astro-ph/0405183v1.

[2] C. Lonsdale, "Generation of a Site Mask from Aerial Photography," internal report, http://mwa-lfd.haystack.mit.edu/twiki/bin/view/Main/MWAtechnicalMemoSeries/, 2008

[3] Q. Wang, O. Ronneberger, and H. Burkhardt, Fourier Analysis in Polar and Spherical Coordinates, internal report, http://lmb.informatik.uni-freiburg.de/papers/, 2008.

# A Calculations

Here we define some mathematical functions used in the text. We start by defining $b_{array}(r, \phi)$ and $b_{ideal}(r, \phi)$ as the basline distributions of a sample realization and the ideal respectively. Then we define $D(r, \phi) \equiv b_{array}(r, \phi) - b_{ideal}(r, \phi)$. Then we have

$$\chi^2 = \int_0^{2\pi} d\phi \int_0^R dr\ r \left( \frac{D(r, \phi)}{\sigma(r, \phi)} \right)^2 , \tag{1}$$

where $\sigma(r, \phi)$ is the standard deviation for a given baseline in the ideal distribution, and $R$ is the maximum baseline length possible (1.5km on our case).

Next we decompose $D(r, \phi)$ using the eigenfunctions of the Laplacian. Because $D(R, \phi)$ must vanish for all $\phi$, we have a discrete spectrum, and can write

$$D(r, \phi) = \sum_{n=1}^{\infty} \sum_{m=0}^{\infty} J_m(k_{mn} r)(A_{mn} \sin(m\phi) + B_{mn} \cos(m\phi)), \tag{2}$$

where $k_{mn} = x_{mn}/R$, and $x_{mn}$ is the $n$th zero of the $m$th Bessel function. Here we have used the fact that $D(r, \phi)$ is real (and hence $A_{mn}$ and $B_{mn}$ must be real) and non singular. The Fourier coefficients can be found by the orthogonality of the basis functions.

$$A_{mn} = \frac{2}{\pi R^2 J_{m+1}^2(k_{mn} R)} \int_0^{2\pi} d\phi \int_0^R dr\ r D(r, \phi) J_m(k_{mn} r) \sin(m\phi) \tag{3a}$$

$$B_{mn} = \frac{2}{\pi R^2 J_{m+1}^2(k_{mn} R)} \int_0^{2\pi} d\phi \int_0^R dr\ r D(r, \phi) J_m(k_{mn} r) \cos(m\phi) \tag{3b}$$

Any azimuthal asymmetry will be revealed by non-zero coefficients with $m > 0$. Therefore, we define $\zeta$ as the total power outside the $m = 0$ modes.

$$\zeta \equiv \sum_{m>0,n} \sqrt{A_{mn}^2 + B_{mn}^2} \tag{4}$$